Without Tobramycin

With Tobramycin (Number of 40)

Up

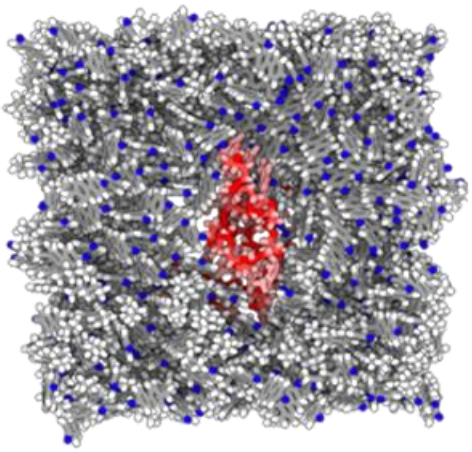

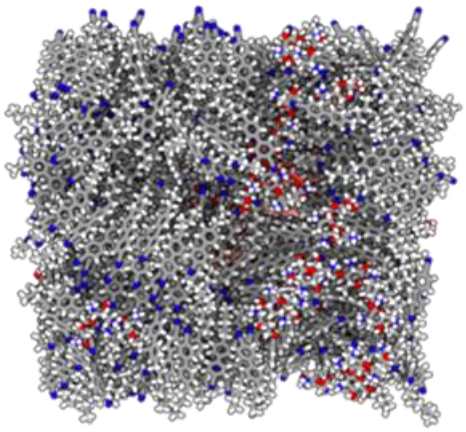

Front

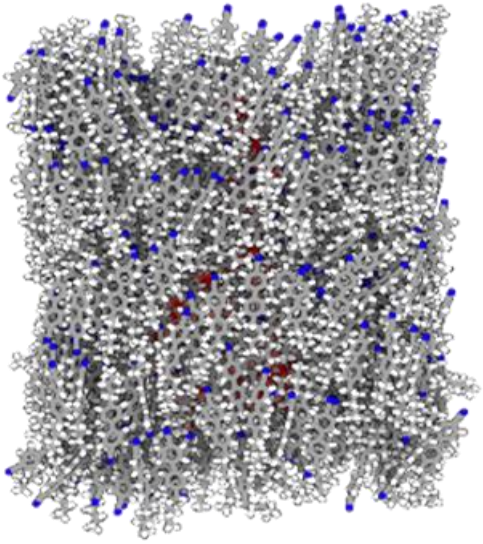

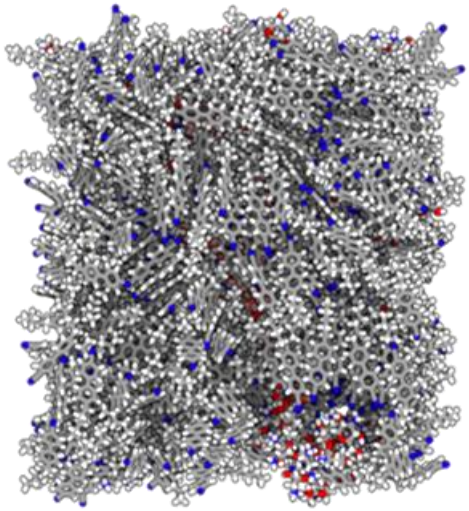

Front

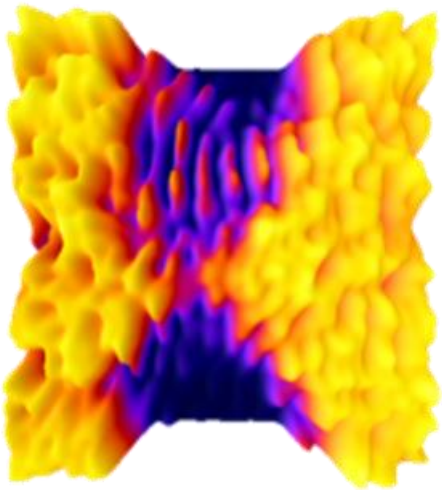

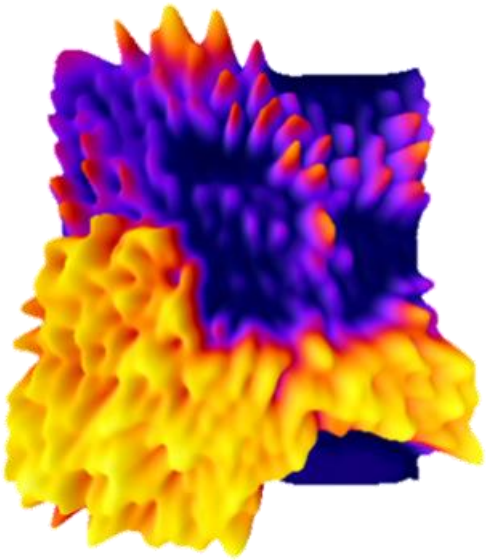

Molecular Dynamics Simulation as a Promising Approach for Computational Study of Liquid Crystal-based Aptasensors

Hamed Zahraee[a,b], Seyed Shahriar Arab[c], Zahra Khoshbin[d,e,*], Seyed Mohammad Taghdisi[a,b], Khalil Abnous[d,e,*]

[a] Targeted Drug Delivery Research Center, Pharmaceutical Technology Institute, Mashhad University of Medical Sciences, Mashhad, Iran

[b] Department of Pharmaceutical Biotechnology, School of Pharmacy, Mashhad University of Medical Sciences, Mashhad, Iran

[c] Department of Pediatrics, University of California, San Diego, La Jolla, CA 92093, USA

[d] Pharmaceutical Research Center, Pharmaceutical Technology Institute, Mashhad University of Medical Sciences, Mashhad, Iran

[e] Department of Medicinal Chemistry, School of Pharmacy, Mashhad University of Medical Sciences, Mashhad, Iran

* Corresponding Authors:

Prof. Khalil Abnous
Professor of Department of Medicinal Chemistry
Pharmaceutical Research Center, School of Pharmacy
Mashhad University of Medical Sciences
Mashhad, Iran
Tel.: +98 5131801112; **FAX**.: +98 5138823251
Email: abnouskh@mums.ac.ir

Dr. Zahra Khoshbin
Pharmaceutical Research Center, Pharmaceutical Technology Institute
Mashhad University of Medical Sciences
Mashhad, Iran
Tel.: +985131801100; **FAX**.: +98511-38823251
Email: khoshbinz991@mums.ac.ir

Abstract

As a potent computational methodology, molecular dynamics (MD) simulation provides advantageous knowledge about biological compounds from the molecular viewpoint. In particular, MD simulation gives exact information about aptamer strands, such as the short synthetic oligomers, their orientation, binding sites, folding-unfolding state, and conformational re-arrangement. Also, the effect of the different chemicals and biochemicals as the components of aptamer-based sensors (aptasensors) on the aptamer-target interaction can be investigated by MD simulation. Liquid crystals (LCs) as soft substances with characteristics of both solid anisotropy and liquid fluidity are new candidates for designing label-free aptasensors. To now, diverse aptasensors have been developed experimentally based on the optical anisotropy, fluidity, and long-range orientational order of LCs. Here, we represent a computational model of an LC-based aptasensor through a detailed MD simulation study. The different parameters are defined and studied to achieve a comprehensive understanding of the computational design of the LC-based aptasensor, including the density of LCs, their orientation angle, and lognormal distribution in the absence and presence of aptamer strands, both aptamer and target molecules with various concentrations, and interfering substance. As a case study, the tobramycin antibiotic is considered the target molecule for the computational model of the LC-based aptasensor.

Keywords: Aptamer; Liquid crystal; Biosensor; MD simulation; Tobramycin; Density

1. Introduction

Biosensors have gained significant attention as highly efficient analytical devices in various fields of science, such as healthcare, pharmaceuticals, clinical diagnostics, environmental monitoring, and food quality control (Azzouz et al., 2022; Khoshbin et al., 2023; Zavvar et al., 2022). Generally, biosensors can include diverse types of bioreceptor segments for the specific targeting of molecules, such as antibodies, peptides, nucleic acids, cells, enzymes, aptamers, and more. Among these, biosensors based on aptamers, known as aptasensors, are some of the most effective and well-organized biosensing tools available (An et al., 2022; Du & Dong, 2017; Hamed Zahraee, Atiyeh Mehrzad, et al., 2023). Aptamers are synthetic single-stranded oligonucleotides that exhibit high binding affinity to a wide range of targets and are obtained through the systematic evolution of ligands by the exponential enrichment (SELEX) selection method (Darmostuk, Rimpelova, Gbelcova, & Ruml, 2015; Ellington & Szostak, 1990). This in-vitro production method eliminates the need for laboratory animals to synthesize aptamers. Moreover, the small size and low weight of aptamers makes their generation and modification facile and cost-effective (Hamed Zahraee, Zahra Khoshbin, et al., 2023). Aptamers possess long shelf life, less immunogenicity and toxicity, great stability, biocompatibility, and reversible thermal denaturation (Keefe, Pai, & Ellington, 2010). These outstanding advantages make aptamers efficacious receptors for diverse biological sensing approaches. Additionally, aptasensors have a fast response time, low cost, and great target detection limit, making them user-friendly analytical tools (Khoshbin, Verdian, Housaindokht, Izadyar, & Rouhbakhsh, 2018; Zhu et al., 2022).

Liquid crystals (LCs) are unique materials composed of aromatic molecules with side chains that exhibit a state between isotropic liquid and crystalline solid (Pilz da Cunha, Debije, & Schenning, 2020). Due to their long-range orientational order, responsiveness to external stimuli, elastic strain, optical anisotropy, and susceptibility to orientation, LCs have become an attractive choice for biosensor design (Devi, Pani, & Pal, 2022; Zahra Khoshbin, Khalil Abnous, Seyed Mohammad Taghdisi, & Asma Verdian, 2021; Pani, Sil, & Pal, 2023). LC-based biosensors are a promising candidate for label-free and portable target monitoring assays, as they enable the detection of targets through visualizing the orientation of the LCs using a polarized optical microscope, without the need for labeled probes that can be costly and time-consuming (Hussain, Pina, & Roque, 2009; Jang et al., 2005; Verdian, Rouhbakhsh, & Fooladi, 2021; Y. Wang, Hu, Tian, Gao, & Yu, 2016).

Molecular dynamics (MD) simulation is a potent computational methodology that provides valuable knowledge of biological components (M.-R. Li, Zhang, & Zhang, 2018; Monti,

Cappelli, Bronco, Giusti, & Ciardelli, 2006; Nicholls et al., 2009; Plattner, Doerr, De Fabritiis, & Noe, 2017; Zahraee, Arab, Khoshbin, & Bozorgmehr, 2023). By simulating the molecular interactions in a biological system, MD simulation can provide accurate information about binding sites, structural rearrangements, and the folding-unfolding status of aptamers (Bini, Mascini, Mascini, & Turner, 2011; Gao et al., 2016; Kim, Rhee, & Shin, 2018; Luo & Mu, 2016; Mary, Haris, Varghese, Aparna, & Sudarsanakumar, 2017; Phanchai, Srikulwong, Chompoosor, Sakonsinsiri, & Puangmali, 2018). Additionally, MD simulation can be used to study the dynamics, structure, and energetics of biological systems under a range of experimental conditions, including pressure, pH, and temperature (Aho et al., 2022; Johnson, Kohlmeyer, Johnson, & Klein, 2009; Moradi, Shareghi, Saboury, & Farhadian, 2020; Pal, Aich, Chakraborty, & Jana, 2022). MD simulation can complement experimental methods by preventing incorrect interpretations of experimental results (Cao et al., 2017; Khanniche et al., 2017; Kutnowski et al., 2018; Zahraee, Mohammadi, Parvaee, Khoshbin, & Arab, 2023; Zeng et al., 2016). Moreover, it can provide basic information at the atomistic level when experimental assays have limitations or are incapable (Nada & Furukawa, 2012; Rigoldi et al., 2016; Shao et al., 2021; J. Wang, Qian, Li, & Qiu, 2020).

In this study, we emphasize the potency of MD simulation as a complement to experimental assays in designing an LC-based aptasensor. Specifically, we present a computational model of an LC-based aptasensor through a detailed MD simulation study. As a case study, we selected the tobramycin antibiotic as the target molecule. Tobramycin as an anti-infective antibiotic drug commonly utilizes for therapeutic and prophylactic purposes, because of its good water-solubility, low cost, and antimicrobial effects (DiCicco, Duong, Chu, & Jansen, 2003; Rosalia et al., 2022). However, its abuse can cause adverse effects in human bodies, such as neuromuscular blocking, nephrotoxicity, and hypersensitivity (Ma, Wang, Jia, & Xiang, 2018; Shang et al., 2019; S. Wang et al., 2019). To date, several strategies have been applied to detect tobramycin, including high-performance liquid chromatography, UV-Visible absorption spectroscopy, liquid chromatography-mass spectrometry, and capillary electrophoresis (Blanchaert, Huang, Wach, Adams, & Van Schepdael, 2017; Law et al., 2006; Meng et al., 2021; Mukhtar, Mamat, & See, 2018). Since the methods are time-consuming, high-cost, and operator-dependent, the LC-based aptasensors have been developed for target detection (D. Li et al., 2022; Zhang, Li, Han, Yuan, & He, 2022). However, LC-based aptasensors are impaired by high temperatures and light, leading to a loss of the LCs' contrast (O'Neill & Kelly, 2003; Pagano-Stauffer, Johnson, Clark, & Handschy, 1986). Hence, we emphasize the potency of MD simulation as a complement to experimental assays in studying

an LC-based aptasensor. Indeed, a MD simulation study of LC-based aptasensors can reduce the cost and time of experimental research.

2. Computational Details

The crystal structure of tobramycin and specific aptamer was taken from the protein data bank (PDB ID: 1LC4) to construct the MD input files. The sequence of 5´-ACT TGG TTT AGG TAA TGA GTA-3´ was obtained through nucleotide exchange by YASARA software (Krieger & Vriend, 2014) and modification of hydrogen deficiency using PyMOL software (The PyMOL Molecular Graphics System, Version 1.7.2.1 Schrödinger, LLC.) (DeLano, 2002). Since the orientation of LCs can be easily disrupted by aptamer sequences with more than 24 base units (Z. Khoshbin, K. Abnous, S. M. Taghdisi, & A. Verdian, 2021), two adenosine (A) nucleotides were added to the 3´ end of the aptamer as the spacer. The MD simulations were carried out by GROMACS 2020.2 (Abraham et al., 2015) with the standard CHARMM27 force field (Brooks et al., 2009; Patel, Mackerell, & Brooks, 2004). The structure of 4-Cyano-4'-pentylbiphenyl (5CB) LC was drawn by ChemDraw software (Z. Li, Wan, Shi, & Ouyang, 2004). Its structural and energetic optimization was done by Chem3D (Z. Li et al., 2004) and Gaussian 09 software (Frisch, 2009) by DFT (B3LYP) method within the 6-31++G(2d,2p) basis set. The topology parameters for tobramycin and LC were obtained by using SwissParam server (Zoete, Cuendet, Grosdidier, & Michielin, 2011). Six rectangular boxes were designed in which the aptamers were fixed on their bottom. One system was considered as the control with no tobramycin molecule. Another box was considered for the interfering system containing 5 gentamycin molecules as the interfering compound. Four others included 1, 5, 20, and 40 tobramycin molecules. The boxes were filled with 450 LC molecules. Charge neutrality was done by adding an adequate number of Na^+ and Cl^- ions to the boxes. The details of the simulated systems is given in Table 1. Simulations were carried out using a cut-off distance of 1.4 nm with a time step of 1 fs. The steepest-descent algorithm (Fletcher & Powell, 1963) was applied to minimize the energy of the system. The velocity rescaling thermostat and Parrinello-Rahman barostat were applied for the temperature and pressure coupling, respectively (Bussi, Donadio, & Parrinello, 2007; Parrinello & Rahman, 1981). Periodic boundary conditions (PBC) were introduced in all directions to implement the MD simulations. Finally, 180 ns production MD simulation of each system was performed with a time step of 1 fs at 300 K. The Particle Mesh Ewald (PME) method was considered to obtain the long-range electrostatic interactions (Darden, York, & Pedersen, 1993).

3. Results and Discussions

To introduce MD simulation as a potent approach for computational model of LC-based aptasensor, six different systems were designed and studied by MD simulation, including 1) control system containing fixed tobramycin aptamer at the bottom of simulation box and LCs, 2) interfering system containing fixed tobramycin aptamer, LCs, and 5 gentamycin molecules, 3) target systems containing fixed aptamer, LCs, and tobramycin molecules with the number of 1, 5, 20, and 40 (named A1T, A5T, A20T, and A40T, respectively).

The structural stability of the studied systems was investigated by analyzing the root mean square deviation (RMSD). Figure 1A indicates the RMSD plots of the simulated systems, proving that they were in the equilibration state after the MD simulation. Moreover, 180 ns was considered as the proper time for having precise results from further analyses. The results clarify the greater stability of all the target systems in comparison with both the control and interfering systems.

Root mean square fluctuation (RMSF) is a criterion for conformational flexibility of DNA strands over the simulation time (Chakraborty, Khatua, & Bandyopadhyay, 2016; M. Li et al., 2013). The RMSF plot for the aptamer in the absence and presence of the different numbers of tobramycin, and also, in the presence of interfering compound was depicted against the residue numbers during the MD simulation time in Figure 1B. As it is obvious, the aptamer flexibility decreased in some residues with increasing the number of tobramycin molecules in the systems, which may be due to more interaction of the aptamer with the target molecules. Generally, the middle nucleotides of the aptamer possessed less flexibility than the terminal ones in the systems including targets. Figure 1C indicates the frequency of RMSF for the simulated systems in the range of 0.15-0.45 nm.

Figure 2 indicates the situation of the LC molecules in the different simulated systems in the last frame of the MD simulation. As shown in Figure 2, LCs were in the same direction with the vertical alignment in the control system free of tobramycin, proving the capability of the aptamer strand with nucleotides lower than 24 to regularly align LCs.

The diffusion coefficient (D) parameter can reflect the flexibility of the aptamer that affects the regularity of LCs during the MD simulation. Figure S1 illustrates the remarkable difference in the D parameter of the systems in the absence and presence of tobramycin. According to Figure S1, the D parameter in the control and interfering systems was less than the others, highlighting the less flexibility of the aptamer, and therefore, vertical alignment of LCs. Proximity of the D parameter of interfering system to the control system clarifies a negligible flexibility of the aptamer through no interaction with gentamycin molecules, and therefore,

vertical alignment of LCs in this system. The results indicate that D parameter for the aptamer enhanced with increasing the number of tobramycin molecules in the studied systems. It proves an increase in the aptamer flexibility with increasing the number of tobramycin molecules. Thus, an increased value of the D index proved the greater irregularity in the vertical orientation of LCs.

To have a detailed insight into the state of the LC molecules for each studied system, their angle changes with respect to the Z axis of the simulation box were investigated. For this purpose, a vertical vector was defined as a basis for the initial state of the LC molecules by considering their C12 and N atoms of the nitrile group (Figure 3A); and its angle with the Z axis of the simulation box. Figure 3B indicates the average of the angle of LCs during 180 ns. It is obvious that the changes in the LCs' angle were the least for the control system and system containing gentamycin. Besides, the angle changes for these two systems were the same at the last times of the simulation, proving the negligible disruption of the LCs' alignment in the presence of gentamycin, and also, insignificant interaction of gentamycin with the aptamer. A comparison between the control system and A1T proved that the aptamer-target interaction disturbed the orientation of LC molecules. However, increasing the number of tobramycin molecules to 5 (A5T system) had no considerable effect on the orientation of LCs compared to the A1T system. This confirms that the aptamer binds to tobramycin in a 1:1 stoichiometry, as previously determined in other studies (Vicens & Westhof, 2002; Y. Wang, Killian, Hamasaki, & Rando, 1996). Moreover, an increase in the number of tobramycin molecules to 20 and 40 changed the orientation of LCs. Since the binding stoichiometry of the aptamer to tobramycin was 1:1, the more disruption in the LCs' orientation in the A20T and A40 systems in comparison with the A1T system was due to the free tobramycin molecules. Having difference with this study, in the experimentally-constructed LC-based aptasensors, the free target molecules are eliminated from the aptasensing system during the washing process, and after that, LCs are injected onto the aptasensing substrate. Hence, what causes the change in the vertical arrangement of LCs in the experimental LC aptasensors is only the target molecules interacted with the aptamer strands. Our theoretical results highlight the importance of washing process in the experimentally-constructed LC-based aptasensors to eliminate the undesirable effect of free targets on the order of LCs. The result clarifies that MD simulation can be complementary to experimental assays for designing LC-based aptasensors.

Figure 4 shows the average of the LCs' angle respect to the Z axis for each LC molecule in the simulated systems during the MD simulation. According to Figure 4, in the control system, most of LC molecules possessed an angle of 30° and some of them had a rotation of almost

180° compared to the Z axis, proving their relatively vertical direction. A similar result was obtained for the interfering system, which confirmed no interaction of gentamycin molecule with the aptamer, and consequently, its high specificity toward tobramycin. In A1T system, the number of LCs with the angle more than 60° increased compared to the control system, indicating the specific interaction of the aptamer with tobramycin molecule. With increasing the number of tobramycin molecules, the angle of LCs enhanced from 30° to the range of 60-120°, which showed the disruption of LCs' regularity caused by free tobramycin molecules based on 1:1 aptamer-tobramycin binding stoichiometry. For simplification in a display, the angle of LCs at the first, middle, and end of the simulation time was given in Figure S2, which clearly shows the increase in the changes of the LCs' angle by enhancing the number of tobramycin molecules in the system.

For further confirmation of the accuracy of the results, the lognormal distribution (Kissell & Poserina, 2017) as a continuous probability distribution of the data was applied based on the following equation:

$$Y=(A/X)*\exp(-0.5*(\ln(X/GeoMean)/\ln(GeoSD))^2)$$

in which Y and X are the probability and angle, respectively. A is related to the amplitude and area of the distribution. GeoMean and GeoSD refer to the geometric mean and geometric standard deviation factor, respectively. Table S1 represents the details and results of the lognormal distribution for the studied systems.

Figure 5 indicates the angle probability of LC molecules along with the lognormal distribution during the MD simulation. The results highlight that the maximum probability was less than 30° in the control system and system containing gentamycin, clarifying the slight deviation of LCs from the vertical direction. With adding tobramycin to the system, the probability partly shifted to 30° due to the aptamer-target interaction. With increasing the number of tobramycin molecules from 1 to 40, a considerable shift in the angle probability to near 90° was achieved, highlighting the change in the direction of LCs from vertical close to horizontal. Also, there was a little probability for the angles in the range of 160°-180°, which was related to the LC molecules with a rotation of almost 180° compared to the Z axis. The results of the lognormal distribution were very close to the probability obtained from the MD output, proving the reliability of the MD results. Moreover, the R-squared values from the lognormal analysis were a confirmation for the accuracy of the MD study.

Figure 6 indicates the density of LCs along the X axis in the simulated systems at the initial (0-10 ns), middle (85-95 ns), and end (170-180 ns) of the simulation time. Obviously, the

density of LCs changed with passing of the simulation time. For the control and interfering systems, the changes in the density were almost similar; and slightly increased at the end of the MD simulation. In the systems containing tobramycin molecule, the changes in the density of LCs were significant during the MD simulation. An increase in the density of LCs was observed at the end of the MD simulation compared to that for the control system. A comparison between the density of LCs in A1T, A5T, A20T, and A40T systems highlights the significant perturbation in the LCs' alignment in the presence of more numbers of the target.

The Radial distribution function (RDF) analysis for the studied systems was obtained between the atoms of LCs. Figure S3 indicates that the distance of the C16-C16 atoms of LCs enhanced with increasing the number of the target molecules, due to the more rotation of LCs and greater perturbation of their vertical direction. A comparison with the control system displays that the distance of C16-N atoms of LCs decreased with increasing the number of tobramycin molecules, because of the higher rotation of LC molecules from the vertical state.

Finally, the distance between the aptamer nucleotides and tobramycin molecules was calculated for the last 10 ns of the MD simulation (Figure 7). The distance between the target molecule and aptamer nucleotides can be a criterion for the effective interactions between them. In A1T system, the aptamer nucleotides with the index of 7-14 possessed less distance from tobramycin, and therefore, more effective interaction with it. Hence, their distance from the target molecule (1.2 nm and less than that) was chosen as a criterion for specifying the effective binding sites of the aptamer for tobramycin. In A5T system, tobramycin molecules with the index of 1, 4, and 5 had greater interaction with the middle nucleotides of the aptamer, and those with the index of 2 and 3 possessed more effective interactions with the terminal ones. However, only tobramycin with the index of 4 had a distance of 1.2 nm and less from the nucleotides of 7-14 similar to that for A1T system. The result was in accordance with the previous ones corresponding to the 1:1 aptamer-tobramycin binding stoichiometry. For A20T and A40T systems, some tobramycin molecules possessed a distance of 1.2 nm and less from the aptamer nucleotides. However, tobramycin molecules with the index of 1 and 37 in A20T and A40T systems, respectively, occupied the nucleotides with the index of 7-14. Consequently, the aptamer nucleotides with the index of 7-14 could be specified as the binding sites of tobramycin.

4. Conclusion

In this research, we studied the potency of MD simulation to computationally model an LC-based aptasensor for the first time. As a case study, the tobramycin antibiotic has been chosen as the target molecule. 180 ns MD simulation was done for the control system, interfering system having gentamycin, and four systems with the different concentrations of tobramycin (A1T, A5T, A20T, and A40T). RMSD results proved the structural stability of the simulated systems after the MD simulation. RMSF analysis indicated that the aptamer flexibility decreased in some residues with increasing the number of tobramycin, which may be due to more interaction of the aptamer with the target molecules. The basis of the LC-aptasensor is change of the vertical alignment of LCs to random in the presence of the target, due to the aptamer-target interaction. Besides, the more aptamer-target complexes, the higher disruption of the vertical arrangement of LCs is. The visualization of the last frame of the simulated systems by PyMOL software indicated that LCs were in the same direction with the vertical alignment in the control system free of tobramycin as well as the interfering system; while the presence of tobramycin molecule significantly disrupted the vertical regularity of LCs. The observations were in accordance with the experimental results (Zahra Khoshbin et al., 2021; Rouhbakhsh, Verdian, & Rajabzadeh, 2020). A detailed insight was achieved by investigating the average of the angle of LCs during 180 ns. The changes in the LCs' angle were negligible in the control and interfering systems, proving an insignificant interaction of gentamycin with the aptamer. The average of the angle increased in A1T system that confirmed the significant changes in the vertical alignment of LCs due to the great specific interaction of the aptamer with the target. With increasing the number of tobramycin molecules from 1 to 40, a great shift in the angle probability to near 90° was achieved, proving the change in the direction of LCs from vertical close to horizontal. Based on 1:1 aptamer-tobramycin binding stoichiometry, the disruption of LCs' regularity in A5T, A20T, and A40T systems was induced by free tobramycin molecules. The density of LCs in the systems containing tobramycin remarkably changed during the MD simulation. A comparison between the density of LCs in A1T, A5T, A20T, and A40T systems proved the significant irregularity in the LCs' alignment in the presence of more numbers of the target. The study confirmed the potency of MD simulation for study of the LC including biosystems. Besides, LC-based aptasensors can be computationally designed by MD simulation and establishing a relationship between the MD-output parameters, such as the density of LCs and their angle change, with the concentration of the desired target.

Conflicts of Interest

The author(s) declare that they have no competing interests.

Acknowledgment

Financial support for this study was provided by Mashhad University of Medical Sciences. We also thank Mr. Ali Akbar Bromideh (Faculty of Mathematical Sciences, Shahid Beheshti University, Tehran, Iran) for providing statistical support.

References

Abraham, M. J., Murtola, T., Schulz, R., Páll, S., Smith, J. C., Hess, B., & Lindahl, E. (2015). GROMACS: High performance molecular simulations through multi-level parallelism from laptops to supercomputers. *SoftwareX, 1-2*, 19-25. doi: 10.1016/j.softx.2015.06.001

Aho, N., Buslaev, P., Jansen, A., Bauer, P., Groenhof, G., & Hess, B. (2022). Scalable Constant pH Molecular Dynamics in GROMACS. *J Chem Theory Comput, 18*(10), 6148-6160. doi: 10.1021/acs.jctc.2c00516

An, J. E., Kim, K. H., Park, S. J., Seo, S. E., Kim, J., Ha, S., . . . Kwon, O. S. (2022). Wearable Cortisol Aptasensor for Simple and Rapid Real-Time Monitoring. *ACS Sens, 7*(1), 99-108. doi: 10.1021/acssensors.1c01734

Azzouz, A., Hejji, L., Kim, K. H., Kukkar, D., Souhail, B., Bhardwaj, N., . . . Zhang, W. (2022). Advances in surface plasmon resonance-based biosensor technologies for cancer biomarker detection. *Biosens Bioelectron, 197*, 113767. doi: 10.1016/j.bios.2021.113767

Bini, A., Mascini, M., Mascini, M., & Turner, A. P. (2011). Selection of thrombin-binding aptamers by using computational approach for aptasensor application. *Biosens Bioelectron, 26*(11), 4411-4416. doi: 10.1016/j.bios.2011.04.053

Blanchaert, B., Huang, S., Wach, K., Adams, E., & Van Schepdael, A. (2017). Assay Development for Aminoglycosides by HPLC with Direct UV Detection. *J Chromatogr Sci, 55*(3), 197-204. doi: 10.1093/chromsci/bmw169

Brooks, B. R., Brooks, C. L., 3rd, Mackerell, A. D., Jr., Nilsson, L., Petrella, R. J., Roux, B., . . . Karplus, M. (2009). CHARMM: the biomolecular simulation program. *J Comput Chem, 30*(10), 1545-1614. doi: 10.1002/jcc.21287

Bussi, G., Donadio, D., & Parrinello, M. (2007). Canonical sampling through velocity rescaling. *The Journal of chemical physics, 126*(1), 014101

Cao, L.-R., Zhang, C.-Y., Zhang, D.-L., Chu, H.-Y., Zhang, Y.-B., & Li, G.-H. (2017). Recent Developments in Using Molecular Dynamics Simulation Techniques to Study Biomolecules. *Acta Physico-Chimica Sinica, 33*(7), 1354-1365

Chakraborty, K., Khatua, P., & Bandyopadhyay, S. (2016). Exploring ion induced folding of a single-stranded DNA oligomer from molecular simulation studies. *Phys Chem Chem Phys, 18*(23), 15899-15910. doi: 10.1039/c6cp00663a

Darden, T., York, D., & Pedersen, L. (1993). Particle mesh Ewald: An N· log (N) method for Ewald sums in large systems. *The Journal of chemical physics, 98*(12), 10089-10092

Darmostuk, M., Rimpelova, S., Gbelcova, H., & Ruml, T. (2015). Current approaches in SELEX: An update to aptamer selection technology. *Biotechnol Adv, 33*(6 Pt 2), 1141-1161. doi: 10.1016/j.biotechadv.2015.02.008

DeLano, W. L. (2002). Pymol: An open-source molecular graphics tool. *CCP4 Newsl. Protein Crystallogr, 40*(1), 82-92

Devi, M., Pani, I., & Pal, S. K. (2022). Liquid Crystals as Signal Transducers for Sensing of Analytes Using Aptamer as Recognition Probe. *Liquid Crystals Reviews*(just-accepted), 1-41

DiCicco, M., Duong, T., Chu, A., & Jansen, S. A. (2003). Tobramycin and gentamycin elution analysis between two in situ polymerizable orthopedic composites. *J Biomed Mater Res B Appl Biomater, 65*(1), 137-149. doi: 10.1002/jbm.b.10528

Du, Y., & Dong, S. (2017). Nucleic Acid Biosensors: Recent Advances and Perspectives. *Anal Chem, 89*(1), 189-215. doi: 10.1021/acs.analchem.6b04190

Ellington, A. D., & Szostak, J. W. (1990). In vitro selection of RNA molecules that bind specific ligands. *Nature, 346*(6287), 818-822. doi: 10.1038/346818a0

Fletcher, R., & Powell, M. J. (1963). A rapidly convergent descent method for minimization. *The computer journal, 6*(2), 163-168

Frisch, A. (2009). gaussian 09W Reference. *Wallingford, USA, 25p, 470*

Gao, S., Hu, B., Zheng, X., Liu, D., Sun, M., Qin, J., . . . Wang, L. (2016). Study of the binding mechanism between aptamer GO18-Td and gonyautoxin 1/4 by molecular simulation. *Physical Chemistry Chemical Physics, 18*(34), 23458-23461

Hussain, A., Pina, A. S., & Roque, A. C. (2009). Bio-recognition and detection using liquid crystals. *Biosens Bioelectron, 25*(1), 1-8. doi: 10.1016/j.bios.2009.04.038

Jang, C. H., Tingey, M. L., Korpi, N. L., Wiepz, G. J., Schiller, J. H., Bertics, P. J., & Abbott, N. L. (2005). Using liquid crystals to report membrane proteins captured by affinity microcontact printing from cell lysates and membrane extracts. *J Am Chem Soc, 127*(25), 8912-8913. doi: 10.1021/ja051079g

Johnson, R. R., Kohlmeyer, A., Johnson, A. T., & Klein, M. L. (2009). Free energy landscape of a DNA-carbon nanotube hybrid using replica exchange molecular dynamics. *Nano Lett, 9*(2), 537-541. doi: 10.1021/nl802645d

Keefe, A. D., Pai, S., & Ellington, A. (2010). Aptamers as therapeutics. *Nat Rev Drug Discov, 9*(7), 537-550. doi: 10.1038/nrd3141

Khanniche, S., Mathieu, D., Pereira, F., Frenois, C., Colin, D., Barthet, C., & Hairault, L. (2017). Quantitative evaluation of the responses of a gravimetric gas sensor based on mesoporous functionalized silica: Application to 2, 4-DNT and TNT detection. *Sensors and Actuators B: Chemical, 248*, 470-480

Khoshbin, Z., Abnous, K., Taghdisi, S. M., & Verdian, A. (2021). Liquid crystal-based biosensors as lab-on-chip tools: Promising for future on-site detection test kits. *TrAC Trends in Analytical Chemistry, 142*, 116325

Khoshbin, Z., Abnous, K., Taghdisi, S. M., & Verdian, A. (2021). A novel liquid crystal-based aptasensor for ultra-low detection of ochratoxin a using a pi-shaped DNA structure: Promising for future on-site detection test strips. *Biosens Bioelectron, 191*, 113457. doi: 10.1016/j.bios.2021.113457

Khoshbin, Z., Verdian, A., Housaindokht, M. R., Izadyar, M., & Rouhbakhsh, Z. (2018). Aptasensors as the future of antibiotics test kits-a case study of the aptamer application in the chloramphenicol detection. *Biosensors and Bioelectronics, 122*, 263-283

Khoshbin, Z., Zahraee, H., Ramezani, M., Alibolandi, M., Verdian, A., Abnous, K., & Taghdisi, S. M. (2023). Surfactant-regularized liquid crystal aptasensor for optical monitoring of prostate-specific antigen: Appropriate for health care monitoring. *Microchemical Journal, 193*, 109002. doi: 10.1016/j.microc.2023.109002

Kim, H. W., Rhee, Y. M., & Shin, S. K. (2018). Charge-dipole interactions in G-quadruplex thrombin-binding aptamer. *Phys Chem Chem Phys, 20*(32), 21068-21074. doi: 10.1039/c8cp03050b

Kissell, R., & Poserina, J. (2017). Advanced Math and Statistics. In R. Kissell & J. Poserina (Eds.), *Optimal Sports Math, Statistics, and Fantasy* (pp. 103-135): Academic Press.

Krieger, E., & Vriend, G. (2014). YASARA View—molecular graphics for all devices—from smartphones to workstations. *Bioinformatics, 30*(20), 2981-2982

Kutnowski, N., Shmuely, H., Dahan, I., Shmulevich, F., Davidov, G., Shahar, A., . . . Shaanan, B. (2018). The 3-D structure of VNG0258H/RosR–A haloarchaeal DNA-binding protein in its ionic shell. *Journal of structural biology, 204*(2), 191-198

Law, W. S., Kuban, P., Yuan, L. L., Zhao, J. H., Li, S. F., & Hauser, P. C. (2006). Determination of tobramycin in human serum by capillary electrophoresis with contactless conductivity detection. *Electrophoresis, 27*(10), 1932-1938. doi: 10.1002/elps.200500819

Li, D., Ling, S., Meng, D., Zhou, B., Liang, P., & Lv, B. (2022). Sensitive fluorescent aptasensing of tobramycin on graphene oxide coupling strand displacement amplification and hybridization chain reaction. *Int J Biol Macromol, 220*, 1287-1293. doi: 10.1016/j.ijbiomac.2022.08.158

Li, M.-R., Zhang, N., & Zhang, F.-S. (2018). Computational investigation of the conformation transitions of DNA in modified water models. *Journal of Molecular Liquids, 271*, 175-181

Li, M., Shoemaker, B. A., Thangudu, R. R., Ferraris, J. D., Burg, M. B., & Panchenko, A. R. (2013). Mutations in DNA-binding loop of NFAT5 transcription factor produce unique outcomes on protein-DNA binding and dynamics. *J Phys Chem B, 117*(42), 13226-13234. doi: 10.1021/jp403310a

Li, Z., Wan, H., Shi, Y., & Ouyang, P. (2004). Personal experience with four kinds of chemical structure drawing software: review on ChemDraw, ChemWindow, ISIS/Draw, and ChemSketch. *J Chem Inf Comput Sci, 44*(5), 1886-1890. doi: 10.1021/ci049794h

Luo, D., & Mu, Y. (2016). Computational insights into the stability and folding pathways of human telomeric DNA G-quadruplexes. *The Journal of Physical Chemistry B, 120*(22), 4912-4926

Ma, Q., Wang, Y., Jia, J., & Xiang, Y. (2018). Colorimetric aptasensors for determination of tobramycin in milk and chicken eggs based on DNA and gold nanoparticles. *Food Chem, 249*, 98-103. doi: 10.1016/j.foodchem.2018.01.022

Mary, V., Haris, P., Varghese, M. K., Aparna, P., & Sudarsanakumar, C. (2017). Experimental Probing and Molecular Dynamics Simulation of the Molecular Recognition of DNA Duplexes by the Flavonoid Luteolin. *J Chem Inf Model, 57*(9), 2237-2249. doi: 10.1021/acs.jcim.6b00747

Meng, T., Kosmider, L., Chai, G., Moothedathu Raynold, A. A., Pearcy, A. C., Qin, B., . . . Xu, Q. (2021). LC-MS/MS method for simultaneous quantification of dexamethasone and tobramycin in rabbit ocular biofluids. *J Chromatogr B Analyt Technol Biomed Life Sci, 1170*, 122610. doi: 10.1016/j.jchromb.2021.122610

Monti, S., Cappelli, C., Bronco, S., Giusti, P., & Ciardelli, G. (2006). Towards the design of highly selective recognition sites into molecular imprinting polymers: a computational approach. *Biosensors and Bioelectronics, 22*(1), 153-163

Moradi, S., Shareghi, B., Saboury, A. A., & Farhadian, S. (2020). Investigation on the interaction of acid phosphatase with putrescine using docking, simulations methods and multispectroscopic techniques. *Int J Biol Macromol, 150*, 90-101. doi: 10.1016/j.ijbiomac.2020.02.057

Mukhtar, N. H., Mamat, N. A., & See, H. H. (2018). Monitoring of tobramycin in human plasma via mixed matrix membrane extraction prior to capillary electrophoresis with contactless conductivity detection. *J Pharm Biomed Anal, 158*, 184-188. doi: 10.1016/j.jpba.2018.05.044

Nada, H., & Furukawa, Y. (2012). Antifreeze proteins: computer simulation studies on the mechanism of ice growth inhibition. *Polymer Journal, 44*(7), 690-698. doi: 10.1038/pj.2012.13

Nicholls, I. A., Andersson, H. S., Charlton, C., Henschel, H., Karlsson, B. C., Karlsson, J. G., . . . Wikman, S. (2009). Theoretical and computational strategies for rational molecularly imprinted polymer design. *Biosens Bioelectron, 25*(3), 543-552. doi: 10.1016/j.bios.2009.03.038

O'Neill, M., & Kelly, S. M. (2003). Liquid crystals for charge transport, luminescence, and photonics. *Advanced Materials, 15*(14), 1135-1146

Pagano-Stauffer, L. A., Johnson, K. M., Clark, N., & Handschy, M. (1986). Optical logic gates using ferroelectric liquid crystals *Liquid Crystals and Spatial Light Modulator Materials* (Vol. 684, pp. 88-95): SPIE.

Pal, P., Aich, R., Chakraborty, S., & Jana, B. (2022). Molecular Factors of Ice Growth Inhibition for Hyperactive and Globular Antifreeze Proteins: Insights from Molecular Dynamics Simulation. *Langmuir, 38*(49), 15132-15144. doi: 10.1021/acs.langmuir.2c02149

Pani, I., Sil, S., & Pal, S. K. (2023). Liquid Crystal Biosensors: A New Therapeutic Window to Point-of-Care Diagnostics. *Langmuir, 39*(3), 909-917. doi: 10.1021/acs.langmuir.2c02959

Parrinello, M., & Rahman, A. (1981). Polymorphic transitions in single crystals: A new molecular dynamics method. *Journal of Applied physics, 52*(12), 7182-7190

Patel, S., Mackerell, A. D., Jr., & Brooks, C. L., 3rd. (2004). CHARMM fluctuating charge force field for proteins: II protein/solvent properties from molecular dynamics simulations using a nonadditive electrostatic model. *J Comput Chem, 25*(12), 1504-1514. doi: 10.1002/jcc.20077

Phanchai, W., Srikulwong, U., Chompoosor, A., Sakonsinsiri, C., & Puangmali, T. (2018). Insight into the molecular mechanisms of AuNP-based aptasensor for colorimetric detection: a molecular dynamics approach. *Langmuir, 34*(21), 6161-6169

Pilz da Cunha, M., Debije, M. G., & Schenning, A. (2020). Bioinspired light-driven soft robots based on liquid crystal polymers. *Chem Soc Rev, 49*(18), 6568-6578. doi: 10.1039/d0cs00363h

Plattner, N., Doerr, S., De Fabritiis, G., & Noe, F. (2017). Complete protein-protein association kinetics in atomic detail revealed by molecular dynamics simulations and Markov modelling. *Nat Chem, 9*(10), 1005-1011. doi: 10.1038/nchem.2785

Rigoldi, F., Spero, L., Dalle Vedove, A., Redaelli, A., Parisini, E., & Gautieri, A. (2016). Molecular dynamics simulations provide insights into the substrate specificity of FAOX family members. *Molecular BioSystems, 12*(8), 2622-2633

Rosalia, M., Chiesa, E., Tottoli, E. M., Dorati, R., Genta, I., Conti, B., & Pisani, S. (2022). Tobramycin Nanoantibiotics and Their Advantages: A Minireview. *International Journal of Molecular Sciences, 23*(22), 14080

Rouhbakhsh, Z., Verdian, A., & Rajabzadeh, G. (2020). Design of a liquid crystal-based aptasensing platform for ultrasensitive detection of tetracycline. *Talanta, 206*, 120246. doi: 10.1016/j.talanta.2019.120246

Shang, M., Zhang, J., Qi, H., Gao, Y., Yan, J., & Song, W. (2019). All-electrodeposited amorphous MoS(x)@ZnO core-shell nanorod arrays for self-powered visible-light-activated photoelectrochemical tobramycin aptasensing. *Biosens Bioelectron, 136*, 53-59. doi: 10.1016/j.bios.2019.04.019

Shao, Z., Sun, J., Wang, J., Lv, K., Liao, B., Wang, R., & Jiang, H. (2021). Effects of Modified Cellulose on Methane Hydrate Decomposition: Experiments and Molecular Dynamics Simulations. *ACS Sustainable Chemistry & Engineering, 9*(29), 9689-9697. doi: 10.1021/acssuschemeng.1c01495

Verdian, A., Rouhbakhsh, Z., & Fooladi, E. (2021). An ultrasensitive platform for PCB77 detection: New strategy for liquid crystal-based aptasensor fabrication. *J Hazard Mater, 402*, 123531. doi: 10.1016/j.jhazmat.2020.123531

Vicens, Q., & Westhof, E. (2002). Crystal structure of a complex between the aminoglycoside tobramycin and an oligonucleotide containing the ribosomal decoding a site. *Chem Biol, 9*(6), 747-755. doi: 10.1016/s1074-5521(02)00153-9

Wang, J., Qian, Y., Li, L., & Qiu, X. (2020). Atomic Force Microscopy and Molecular Dynamics Simulations for Study of Lignin Solution Self-Assembly Mechanisms in Organic-Aqueous Solvent Mixtures. *ChemSusChem, 13*(17), 4420-4427. doi: 10.1002/cssc.201903132

Wang, S., Li, Z., Duan, F., Hu, B., He, L., Wang, M., . . . Zhang, Z. (2019). Bimetallic cerium/copper organic framework-derived cerium and copper oxides embedded by mesoporous carbon: Label-free aptasensor for ultrasensitive tobramycin detection. *Anal Chim Acta, 1047*, 150-162. doi: 10.1016/j.aca.2018.09.064

Wang, Y., Hu, Q., Tian, T., Gao, Y., & Yu, L. (2016). A liquid crystal-based sensor for the simple and sensitive detection of cellulase and cysteine. *Colloids Surf B Biointerfaces, 147*, 100-105. doi: 10.1016/j.colsurfb.2016.07.059

Wang, Y., Killian, J., Hamasaki, K., & Rando, R. R. (1996). RNA molecules that specifically and stoichiometrically bind aminoglycoside antibiotics with high affinities. *Biochemistry, 35*(38), 12338-12346. doi: 10.1021/bi960878w

Zahraee, H., Arab, S. S., Khoshbin, Z., & Bozorgmehr, M. R. (2023). A comprehensive computer simulation insight into inhibitory mechanisms of EGCG and NQTrp ligands on amyloid-beta assemblies as the Alzheimer's disease insignia. *J Biomol Struct Dyn, 41*(20), 10830-10839. doi: 10.1080/07391102.2022.2158939

Zahraee, H., Khoshbin, Z., Mohammadi, F., Mashreghi, M., Abnous, K., & Taghdisi, S. M. (2023). Three-way junction skeleton biosensors based on aptamers, DNAzymes, and DNA hybridization probes. *TrAC Trends in Analytical Chemistry, 165*, 117160. doi: 10.1016/j.trac.2023.117160

Zahraee, H., Mehrzad, A., Abnous, K., Chen, C.-H., Khoshbin, Z., & Verdian, A. (2023). Recent Advances in Aptasensing Strategies for Monitoring Phycotoxins: Promising for Food Safety. *Biosensors, 13*(1), 56

Zahraee, H., Mohammadi, F., Parvaee, E., Khoshbin, Z., & Arab, S. S. (2023). Reducing the assemblies of amyloid-beta multimers by sodium dodecyl sulfate surfactant at concentrations lower than critical micelle concentration: molecular dynamics simulation exploration. *J Biomol Struct Dyn*, 1-15. doi: 10.1080/07391102.2023.2247086

Zavvar, T. S., Khoshbin, Z., Ramezani, M., Alibolandi, M., Abnous, K., & Taghdisi, S. M. (2022). CRISPR/Cas-engineered technology: Innovative approach for biosensor development. *Biosens Bioelectron, 214*, 114501. doi: 10.1016/j.bios.2022.114501

Zeng, X., Zhang, L., Xiao, X., Jiang, Y., Guo, Y., Yu, X., . . . Li, M. (2016). Unfolding mechanism of thrombin-binding aptamer revealed by molecular dynamics simulation and Markov State Model. *Sci Rep, 6*, 24065. doi: 10.1038/srep24065

Zhang, H. W., Li, H. K., Han, Z. Y., Yuan, R., & He, H. (2022). Incorporating Fullerenes in Nanoscale Metal-Organic Matrixes: An Ultrasensitive Platform for Impedimetric Aptasensing of Tobramycin. *ACS Appl Mater Interfaces, 14*(5), 7350-7357. doi: 10.1021/acsami.1c23320

Zhu, L., Liang, G., Guo, C., Xu, M., Wang, M., Wang, C., . . . Du, M. (2022). A new strategy for the development of efficient impedimetric tobramycin aptasensors with metallo-covalent organic frameworks (MCOFs). *Food Chem, 366*, 130575. doi: 10.1016/j.foodchem.2021.130575

Zoete, V., Cuendet, M. A., Grosdidier, A., & Michielin, O. (2011). SwissParam: a fast force field generation tool for small organic molecules. *J Comput Chem, 32*(11), 2359-2368. doi: 10.1002/jcc.21816

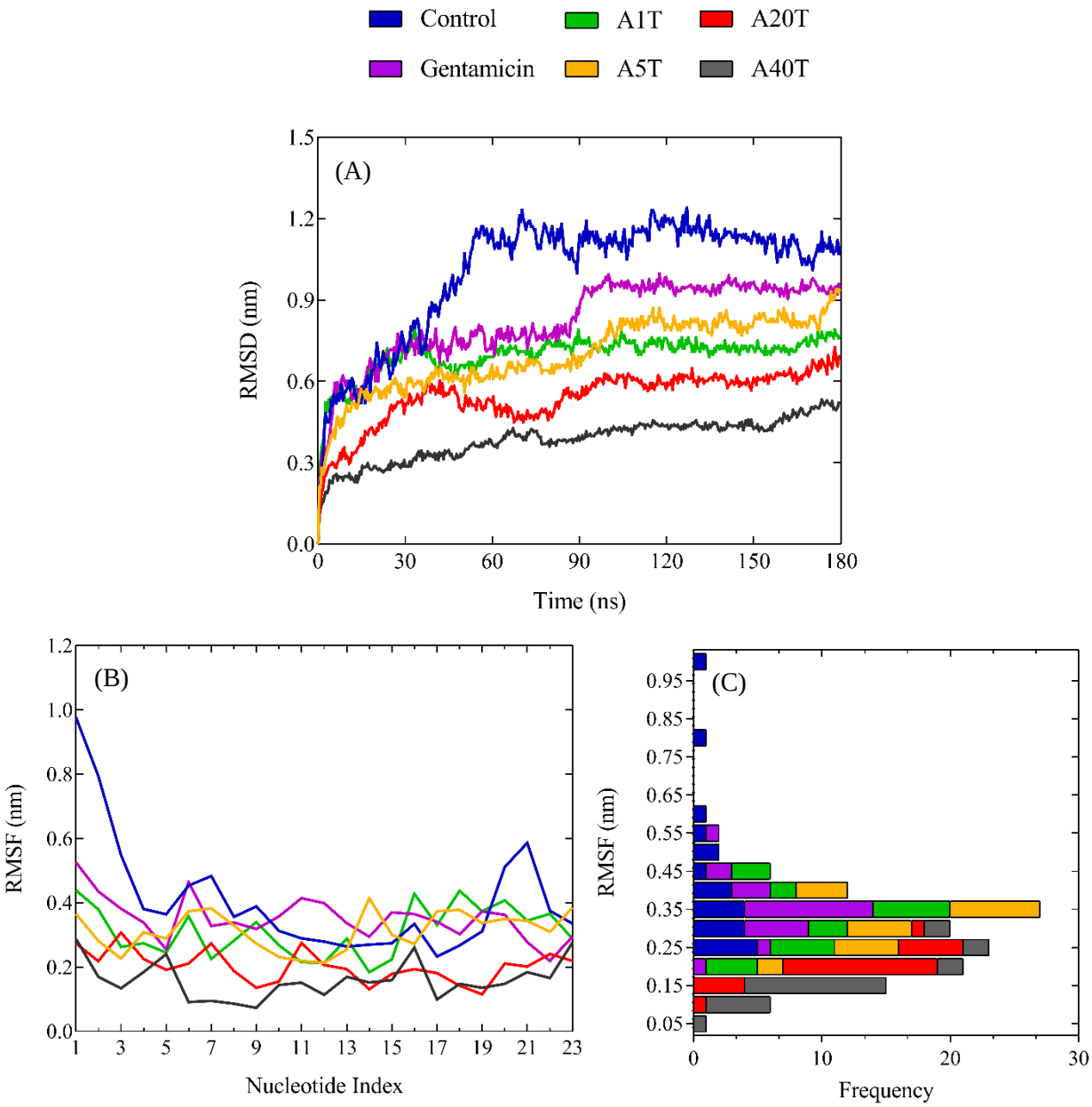

Figure 1. RMSD, RMSF, and RMSF frequency analyses (A-C) for the simulated systems during 180 ns MD simulation.

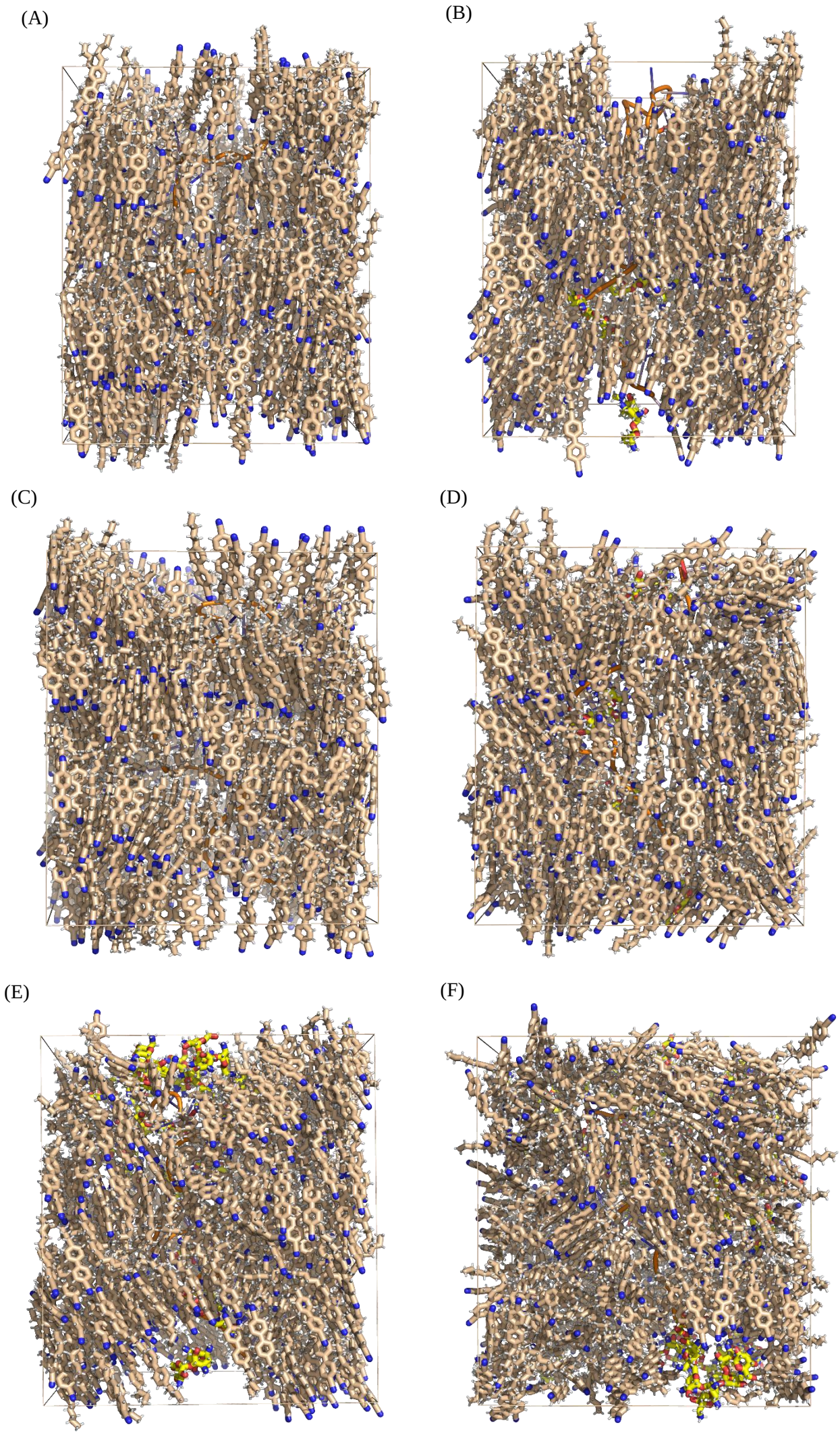

Figure 2. The situation of the LC components of the simulated systems in the last frame of the MD simulation. (A) control system free of tobramycin, (B) system containing gentamycin as the interfering compound, (C-F) systems with 1, 5, 20, and 40 tobramycin molecules, respectively (the phosphate chain of the aptamer is shown to be orange, and the molecule of tobramycin is indicated to be yellow in color).

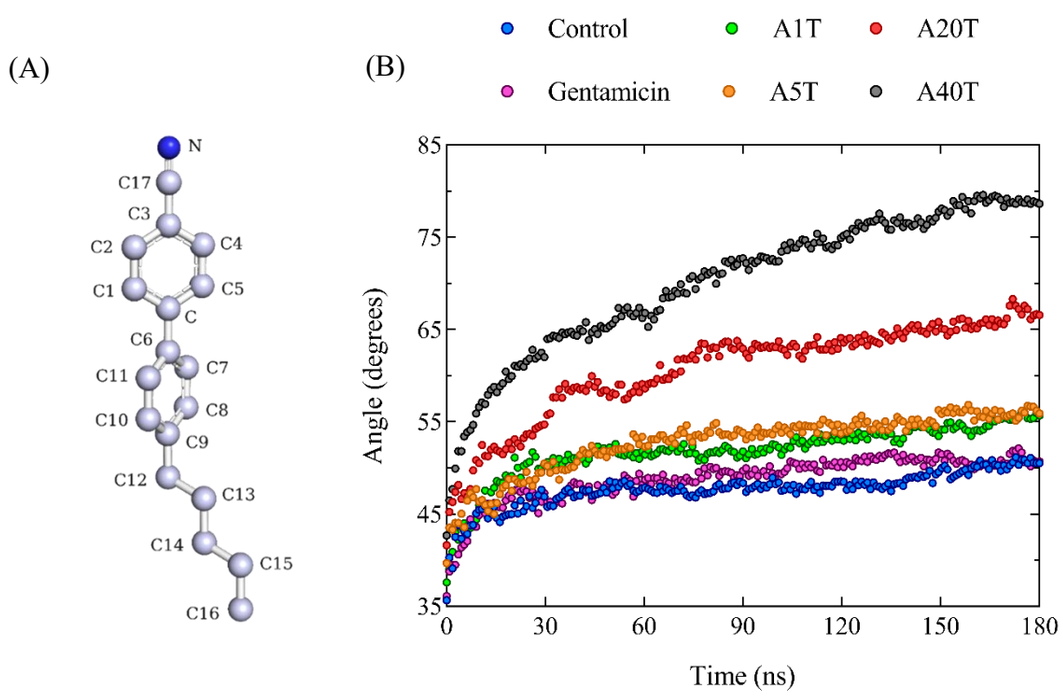

Figure 3. (A) Molecular structure of 4-Cyano-4'-pentylbiphenyl liquid crystal. **(B)** The average of the angles of LC molecules with respect to the Z axis of the simulation box during 180 ns.

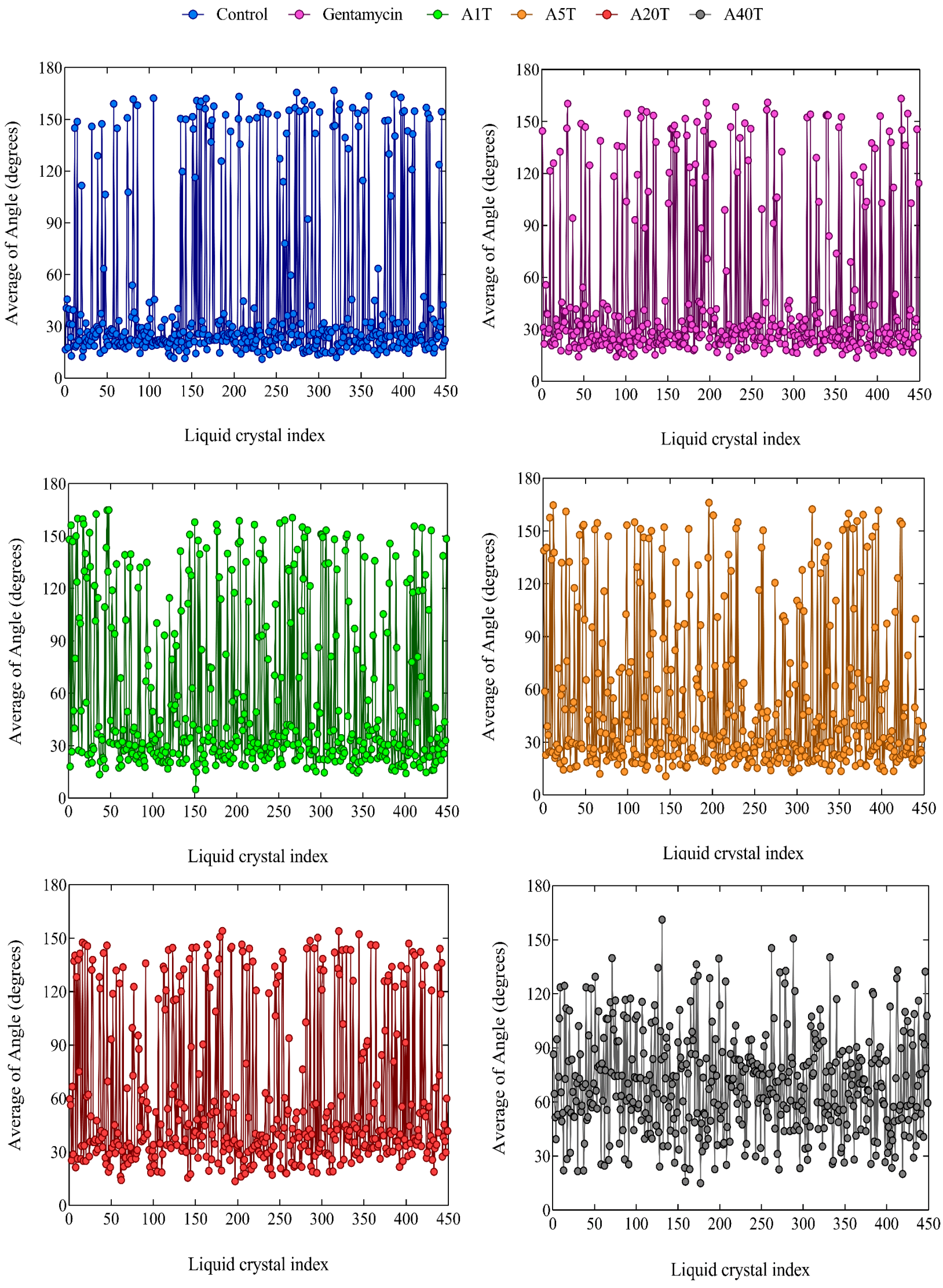

Figure 4. The average of the LCs' angle with respect to the Z axis of the simulation box for each LC molecule in the simulated systems during the MD simulation.

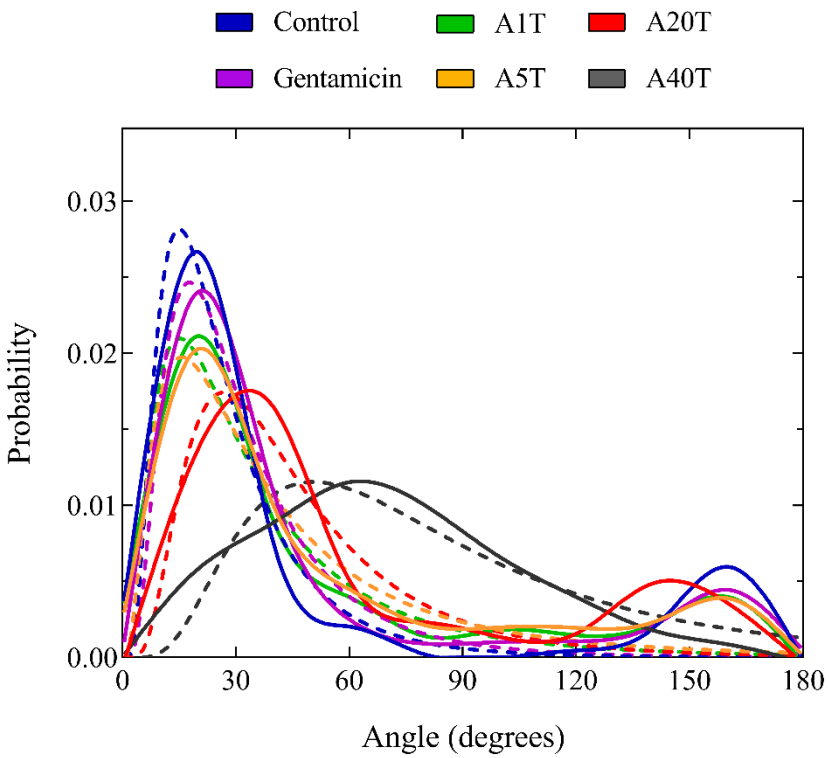

Figure 5. The angle probability of LC molecules was obtained by the lognormal distribution (dashed line) and MD simulation (solid line).

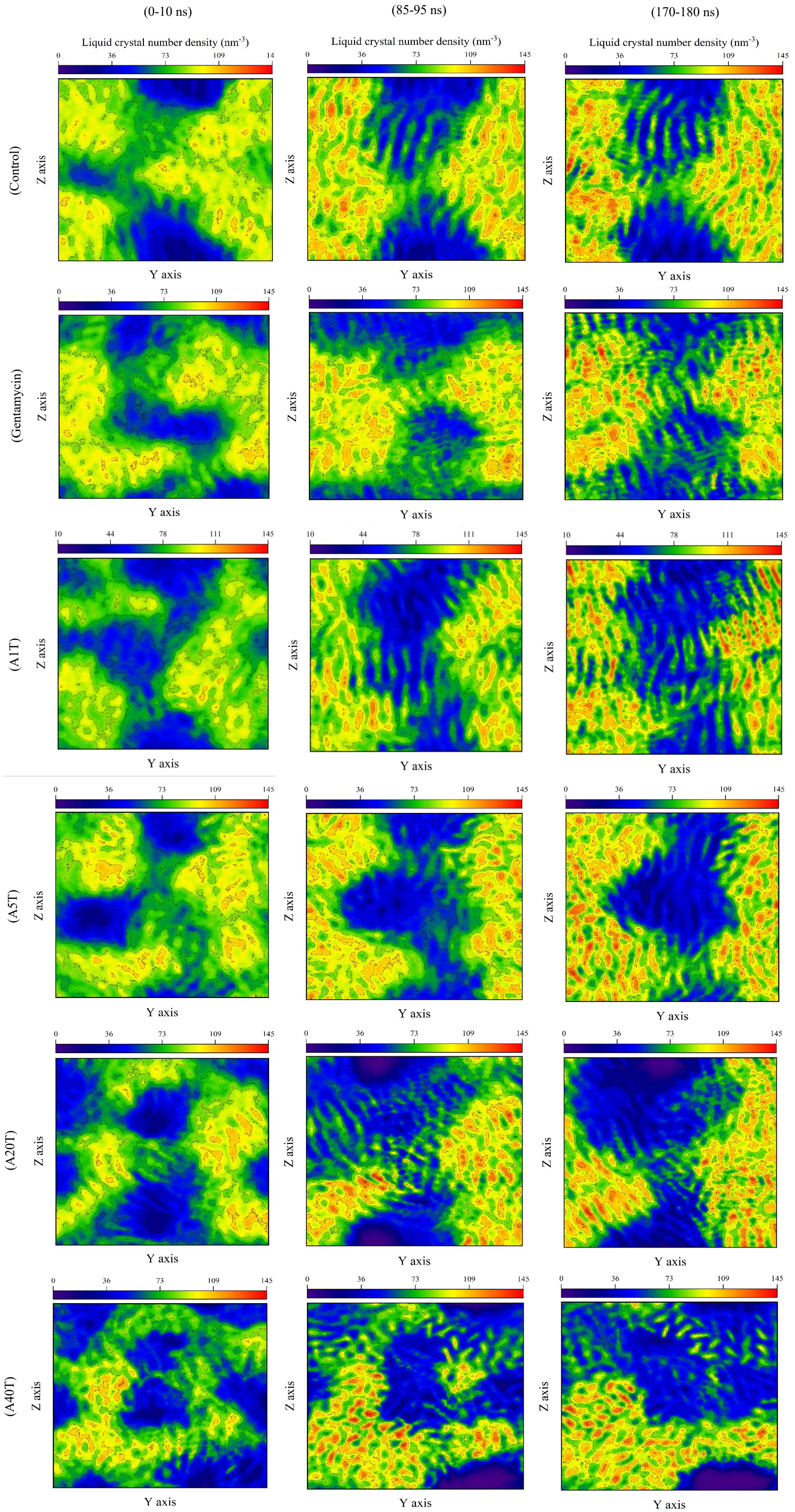

Figure 6. The density (nm^{-3}) graph of the LC molecules along the X axis in the different simulated systems at the initial, middle, and end of the simulation time.

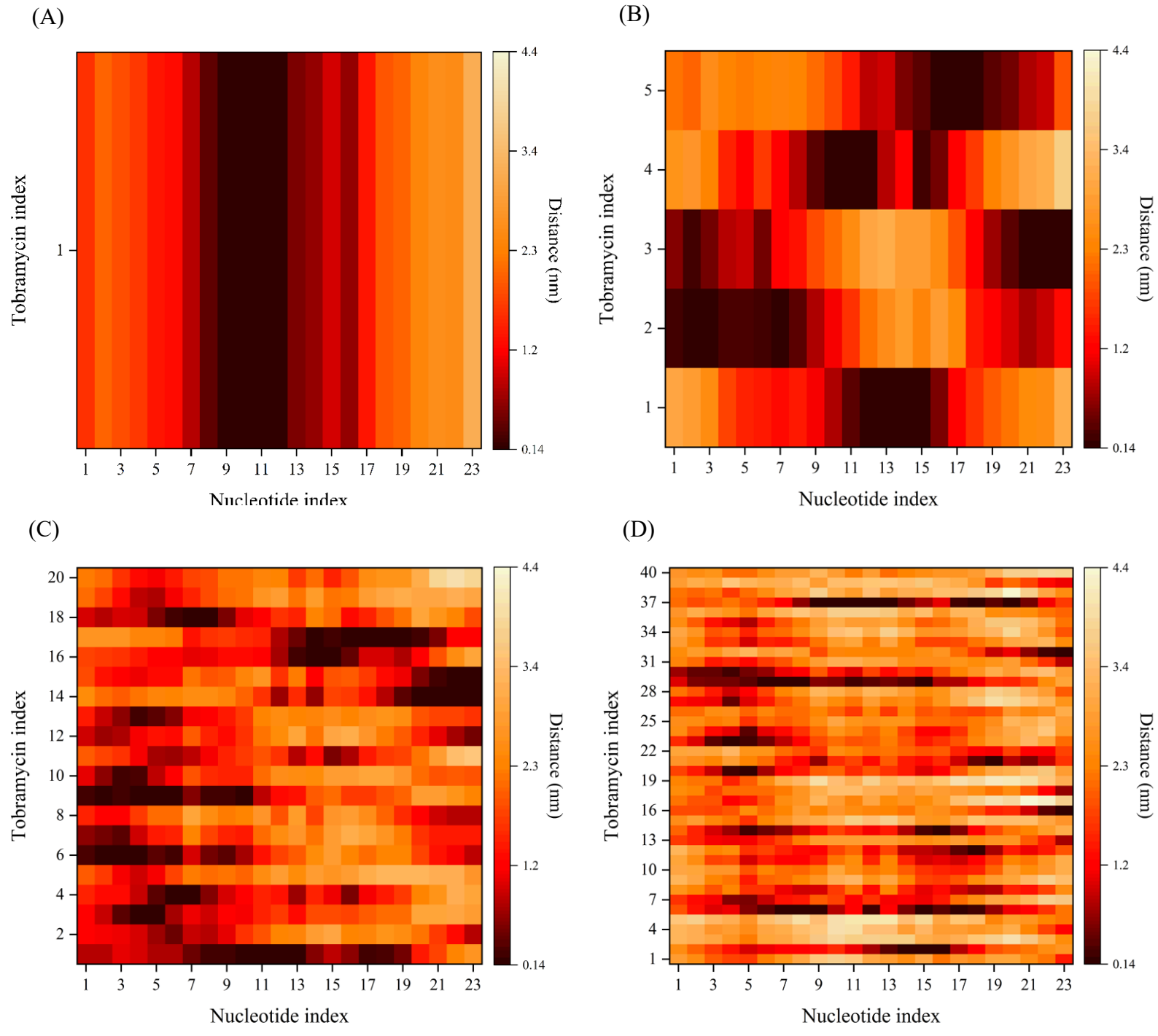

Figure 7. The distance between the tobramycin molecules and the aptamer nucleotides in the A1T, A5T, A20T, and A40T systems (A-D).

Table 1. Details of the simulated systems.

System	No. of Target	No. of LCs	Box Size (nm)	Counterion (Na^+ - Cl^-)	Time (ns)
Aptamer (Control)	0	450	5.6 × 5.6 × 6.7	22 Na^+	180 ns
Aptamer-Gentamycin	5	450	5.7 × 5.6 × 6.8	3 Cl^-	180 ns
Aptamer-Tobramycin	1	450	5.7 × 5.6 × 6.8	17 Na^+	180 ns
	5	450	5.7 × 5.7 × 6.8	3 Cl^-	180 ns
	20	450	5.8 × 6.1 × 6.9	78 Cl^-	180 ns
	40	450	5.8 × 6.3 × 7.0	178 Cl^-	18 ns